

This is a copy of the published version, or version of record, available on the publisher's website. This version does not track changes, errata, or withdrawals on the publisher's site.

6U CubeSat deployable telescope for Earth Observation and astronomical optical imaging

Noah Schwartz, William Brzozowski, Zeshan Ali, Maria Milanova, Katherine Morris, et al.

Published version information:

Citation: N Schwartz et al. 6U CubeSat deployable telescope for optical Earth observation and astronomical optical imaging. In Space Telescopes and Instrumentation 2022: Optical, Infrared, and Millimeter Wave, Montréal, Canada, 17-23 Jul 2022, (2021): 159

DOI: [10.1117/12.2627248](https://doi.org/10.1117/12.2627248)

Copyright 2022 Society of Photo-Optical Instrumentation Engineers (SPIE). One print or electronic copy may be made for personal use only. Systematic reproduction and distribution, duplication of any material in this publication for a fee or for commercial purposes, and modification of the contents of the publication are prohibited.

This version is made available in accordance with publisher policies. Please cite only the published version using the reference above. This is the citation assigned by the publisher at the time of issuing the APV. Please check the publisher's website for any updates.

This item was retrieved from **ePubs**, the Open Access archive of the Science and Technology Facilities Council, UK. Please contact epublications@stfc.ac.uk or go to <http://epubs.stfc.ac.uk/> for further information and policies.

PROCEEDINGS OF SPIE

SPIDigitalLibrary.org/conference-proceedings-of-spie

6U CubeSat deployable telescope for optical Earth observation and astronomical optical imaging

Noah Schwartz, William Brzozowski, Zeshan Ali, Maria Milanova, Katherine Morris, et al.

Noah Schwartz, William Brzozowski, Zeshan Ali, Maria Milanova, Katherine Morris, Charlotte Bond, Jennifer Keogh, Douglas Harvey, Lawrence Bissell, Jean-François Sauvage, Maxime Dumont, Carlos Correia, Phil Rees, Heather Bruce, "6U CubeSat deployable telescope for optical Earth observation and astronomical optical imaging," Proc. SPIE 12180, Space Telescopes and Instrumentation 2022: Optical, Infrared, and Millimeter Wave, 1218031 (27 August 2022); doi: 10.1117/12.2627248

SPIE.

Event: SPIE Astronomical Telescopes + Instrumentation, 2022, Montréal, Québec, Canada

6U CubeSat deployable telescope for Earth Observation and astronomical optical imaging

Noah Schwartz^{*a, c}, William Brzozowski^a, Zeshan Ali^a, Maria Milanova^a, Katherine Morris^a, Charlotte Bond^a, Jennifer Keogh^a, Douglas Harvey^a, Lawrence Bissell^a, Jean-Francois-Sauvage^{b, c}, Maxime Dumont^{b, e}, Carlos Correia^{d, e}, Phil Rees^a, Heather Bruce^a

^aUK Astronomy Technology Centre, Blackford Hill, Edinburgh EH9 3HJ, United Kingdom;

^bONERA, DOTA, F-13661 Salon Cedex Air - France; ^cAix Marseille Univ, CNRS, CNES, LAM, Marseille, France; ^dSpace ODT - Optical Deblurring Technologies, Portugal; ^eINESTEC, FEUP, Porto, Portugal.

ABSTRACT

Available volumes of nanosats such as CubeSats impose physical limits to the telescope diameter, limiting achievable spatial resolution and photometric capability. For example, a 12U CubeSat typically only has sufficient volume to host a 20 cm diameter monolithic telescope. In this paper, we present recent advances in deployable optics to host a 30 cm-diameter telescope in a 6U CubeSat, with a volume of 4U dedicated to the payload and 2U to the satellite bus. To reach this high level of compactness, we fold the primary and secondary mirrors for launch, which are then unfolded and aligned in space. Diffraction-limited imaging quality in the visible part of the spectrum is achieved by controlling each mirror segment in piston, tip, and tilt. In this paper, we first describe overall satellite concept, we then report on the opto-mechanical design of the payload to deploy and adjust the mirrors. Finally, we discuss the automatic phasing of the primary to control the final optical quality of the telescope.

Keywords: Active optics, CubeSat, Co-phasing, Wavefront sensing, Deployable optics.

1 INTRODUCTION

To reach their full potential, many scientific and commercial applications (e.g., climate monitoring and protection, defence and security, time domain astronomy, and solar system exploration) require images at very high-resolution and as often as possible. However, combining both high spatial and temporal resolution is for the moment out of reach at reasonable costs.

This project aims at opening a new parameter space in the trade-off between resolution and revisit time by developing a deployable optical telescope on a CubeSat platform. This breakthrough in performance over current state of the art will provide high-performance payloads - comparable to larger more expensive satellites - while maintaining low-costs. As a comparison, the mass of the SPOT6/7 satellites is 714 kg to achieve 1.5 m Ground Sampling Distance (GSD). This gain in weight directly translates into a gain in cost and therefore allows to multiply the number of platforms and increase the temporal resolution (revisit rate) by a factor 10 to 20.

The telescope will be subject to major perturbations affecting the optical quality: the misalignments introduced by the initial deployment of the optics¹, and the thermo-mechanical deformation of the satellite due varying thermal load^{2, 14}. The very high optical quality required for high angular resolution necessitate the use of an active and autonomous correction to keep the segmented telescope phased to the few-tens nm level^{3, 4}.

In this paper, we present an innovative mechanical design for packaging (fitting into the 4U CubeSat volume), deploying, and controlling the position of the primary mirror petals. We first present section 0 the general concept for achieving high-angular resolution from a CubeSat. In section 3 we report the optical design and discuss the sensitivity to misalignment, a critical aspect to achieve diffraction-limited images in the visible. In section 4, we report key mechanical design features

*noah.schwartz@stfc.ac.uk

and in particular the test of actuators to move individual mirror segments and phase the telescope. Finally in section 5, we report the active optics control.

2 DEPLOYABLE TELESCOPE FOR HIGH-ANGULAR IMAGING IN THE VISIBLE

2.1 Very high angular resolution from a CubeSat

The objective of this technology is to provide very high-angular resolution imaging in the visible at low-cost. This is achieved by folding a large 30cm+ telescope into a small volume - typically in a 6 CubeSat - for launch. The optical elements (segmented primary, secondary mirror, and baffle) are then deployed and aligned once in space. Concepts for deployable secondary mirrors only have been reported⁵, but they can only help stowed volume and cannot improve resolution. In addition, aligning M2 is typically less demanding and requires far less positional precision. We aim to triple the ground resolution (angular resolution) over the current state of the art, with an optical to near-infrared imaging of 1 m GSD from LEO. Owing to their cost advantage, more CubeSats can be placed in a constellation for the same price, leading to more coverage, greater redundancy, and shorter revisit time⁶.

Deployable optics, bringing a 10x cost reduction compared to a non-deployable equivalent, will provide a great potential for creating positive economic and societal transformation, and for addressing various scientific and societal challenges. Figure 2-1 shows an illustration of the deployable space telescope concept, providing higher resolution images of Earth compared to a fixed aperture telescope from the same CubeSat volume.

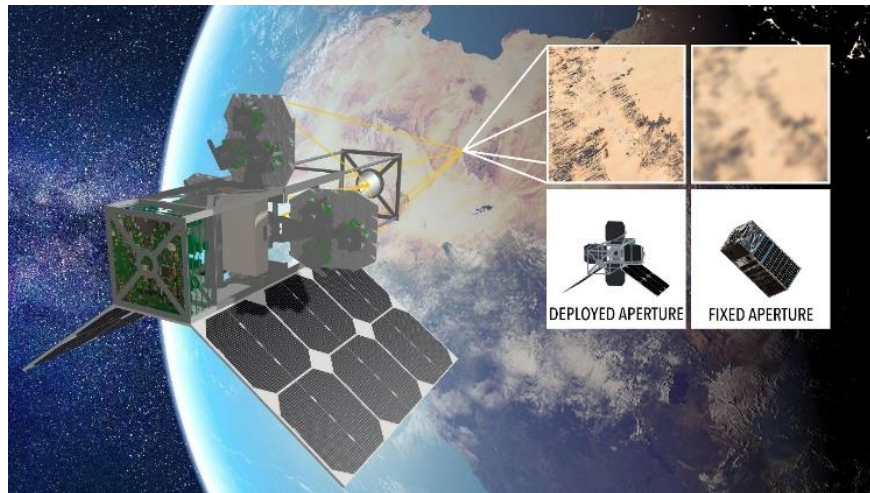


Figure 2-1: Illustration of the deployable space telescope concept, providing higher resolution images of Earth compared to a fixed aperture telescope from the same CubeSat volume.

Many global challenges require a combination of very high-resolution images (i.e., spatial resolution) and high revisit rates (i.e., temporal resolution). Typical examples can be taken from local and urban climate monitoring, civil security, crisis management, flooding (over 75% of natural disasters worldwide involve flooding), and services related to Earth Observation data. However, combining these two requirements is at the moment out of reach at acceptable costs and requires a trade-off between the size and the number of satellites.

In astronomy, high-angular resolution on a CubeSat would also enable the exploration of transient phenomena (e.g., geysers on Enceladus, volcanism on Io), flyby missions (e.g., Comet Interceptor, Discovery), and high spatial and temporal resolution data for solar planets (complementary with HiRISE camera onboard MRO). The better understanding of Mars atmosphere and weather are identified as a strategic knowledge gaps by NASA. Cost-efficient deployable telescope would be a game changer for the preparation for Human exploration, by characterising potential landing sites with high spatial resolution and analysing their evolution over time. Deployable optical satellites may also contribute to monitor and study the Martian local weather effects, in particular the origin of dust storms of small sizes and nucleation of high-altitude clouds. These phenomena are poorly understood today because of the lack of relevant instrumentation. A constellation of 4 to 6 satellites in trailing configuration, in a polar orbit of 400 km could bring the missing information to better understand these transient phenomena.

Beyond Earth observation and astronomy, deployable telescopes are also relevant to LiDAR to increase collecting area and reduce costs. It has been found⁷ that deployable optics would allow a more cost-effective coverage than fixed optics to achieve global coverage within a given timeframe, accounting for loss due to clouds. What is more, the list of potential applications is not limited to those identified above. Evidence of the value of the combined increased temporal and spatial resolution for EO data is exemplified in many publications. They confirm the benefit of detecting daily changes of environmental variables in applications ranging from disease dissemination⁸, the normalised difference vegetation index caused by fires⁹, and surface soil moisture¹⁰.

This work presented in this paper is part of ISAAC (Integrated Space Active Optics for Aberration Compensation), project funded through the United Kingdom Science and Technology Facilities Council STFC.

2.2 Main challenges

The proposed technology - in essence an alternative telescope concept - is composed of deployable structures (primary and secondary mirrors, and baffle), actuators to adjust mirror positions, sensors to measure mirror positions, detector to assess image quality, and onboard active optics to control and adjust mirror positions to reach diffraction-limited image quality. Figure 2-2 shows a simplified illustration of the payload concept. The technology allows a telescope aperture to be larger than the size of the platform. This has two functions; to increase the amount of light entering the telescope and to increase the resolution achievable by the telescope. Telescope resolution is fundamentally limited by the aperture size D (i.e., proportional to λ/D , where λ is the observing wavelength). It should be noted this is a hard science limit rather than a technology limit - new developments in sensor technology make no change to this - it can only be increased by increasing the aperture size.

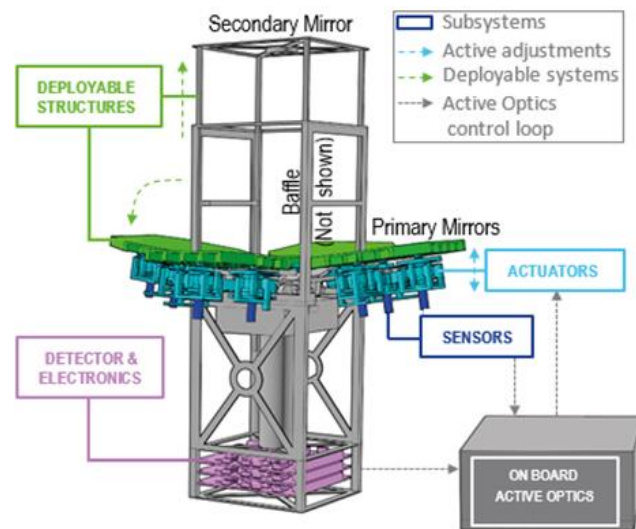


Figure 2-2: Simplified illustration of the payload concept: deployable structures (primary & secondary mirrors, baffle), actuators to adjust mirror positions, sensors to measure mirror positions, detector to assess image quality, and on-board computer to control and adjust mirror positions to reach diffraction-limited image quality (i.e., active optics).

On a conceptual level, deployable optical telescopes are composed of a primary mirror (M1, principal light-gathering surface), a secondary mirror (M2, folding light towards the detector), a baffle to stop unwanted light, and an active optics control system to guarantee optimal optical quality. ATC's initial proof-of-concept developments demonstrated in laboratory that it is possible to fit the mirrors and structure within the very small CubeSat volume, to deploy M1 segments with a precision of several microns, and to control their position with a precision of several tens of nanometres^{11, 12}. We also validated self-alignment procedure using numerical simulations, which now need to be tested in the laboratory. Space qualified actuators to move the mirrors are available commercially, but coupling them to optical surfaces in a precise, reliable, and repeatable manner is challenging. Several key challenges for a deployable telescope from a CubeSat are summarised below:

- Fitting all sub-systems in the extremely tight payload volume (i.e., 4U or approx. 10x20x20 cm³). This is particularly true for the large primary mirror optics which needs to be folded into the volume for launch. Details can be found in section 4).
- Delivering high optical quality in the visible. A detailed optical sensitivity analysis is provided section 3. In addition, in-orbit perturbations (essential due to variations in the thermal load affecting the optical quality of the exposed components) in studied².
- Deploying optical elements such as mirrors accurately, within 10 μm of their optimal position. Initial results have been reported in^{1, 12}.
- Controlling the position of mirrors by moving them by steps typically smaller than 10 nm in the harsh environment of space⁴.
- Removing the human-in-the-loop to align the spacecraft automatically directly in orbit. Additional details are provided section 5 and with the use of machine learning³.

3 OPTICAL DESIGN

3.1 Top level requirements

The telescope has a Cassegrain configuration with a parabolic primary mirror. It will provide 1 m resolution imaging in the visible over a field of 5x5 km² from a 500 km orbit. Table 3-1 provides a short summary of the main relevant requirements.

Table 3-1: Main top-level requirements for the imaging system.

Parameter	Requirement	Comment
Ground Sampling Distance	1 m at 600 nm	The sampling is defined by the pixel footprint on the ground at an operating altitude of 500 km.
Field of View	>2 km (goal 5 km).	With 1 m resolution this corresponds to 5000 pixels.
Wavelengths	<500 nm to >800 nm	Visible part of the spectrum.
Deployment residual wavefront error	<2 waves at 550 nm.	Deployment Alignment Accuracy. The raw (uncalibrated) wavefront error shall be <2 waves at 550 nm
Residual wavefront error	70 nm RMS	Total optical error of the system.
Aperture diameter	≥ 300 mm	To reach a resolution of 1 m on the ground.
M1-M2 distance	≥ 280 mm	increasing M1-M2 distance can have a significant effect on misalignment sensitivity.
Payload volume	4U	6U volume is approx. 100 x 226.3 x 340.5 mm.
Folded optics	Fit inside volume	Polished mirror surface preferably facing toward the interior of the CubeSat for damage protection.

3.2 Optical design

The optical design is a Cassegrain with a field corrector – see Figure 3-1. A Cassegrain design was chosen as, for a longitudinally compact layout, it can achieve a large collecting area and a sufficiently wide and well-corrected field of view. An intermediate focus is created before the field-correcting lenses, which although this results in a relatively fast focal ratio of the telescope and significant primary aberrations, offers at least two necessary benefits. Firstly, that the size of M2 can be minimised – a consequence of a smaller focal length. The diameter of M2 is an important parameter to minimise given the volume constraints of the 6U CubeSat. Specifically, we need to consider the volume the optics occupy when stowed and an M2 larger than 40x40 mm² starts to infringe on mechanical structures. The second benefit of the intermediate focal plane is the control of stray light. Apertures can be placed along the lens barrel at focal and pupil planes, allowing off axis stray light to be easily blocked from reaching the detector.

The optics have been optimised to achieve better than diffraction limited performance at 1 m Ground Sampling Distance (GSD) across the required field of view and wavelength range (Figure 3-3). This design meets these requirements, as well as those listed in 3.1, along with all volume constraints.

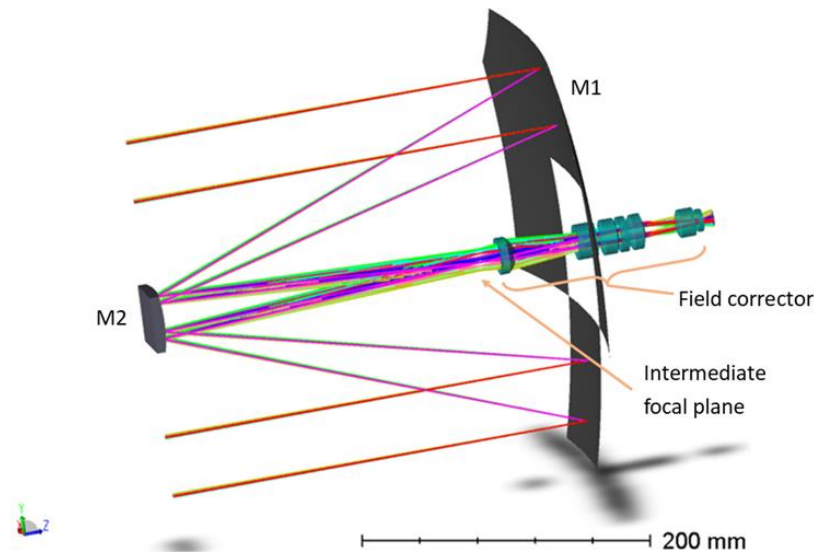


Figure 3-1: Optical layout of ISAAC.

M1 consists of four individual mirror petals, which are to be aligned together to act as a single primary mirror. Figure 3-2 is a wavefront map at nominal alignment, showing the shape of the entrance pupil, with indication of the individual petals. Petal 1 is in a fixed position, whereas petals 2, 3 and 4 are deployable and can be adjusted in flight. The diameter of the aligned M1 is ≥ 300 mm, represented by the white circle. The corners of petals 3 and 4 are clipped, to enable the petals to fit into the stowed CubeSat volume. However, these corners are strictly speaking outside of the required 300 mm pupil diameter and are slightly clipped by the limited M2 size (in particular where the high optical errors are, see Figure 3-2). The remaining area outside the circle adds some resolution in the diagonal direction, where the other corners are missing.

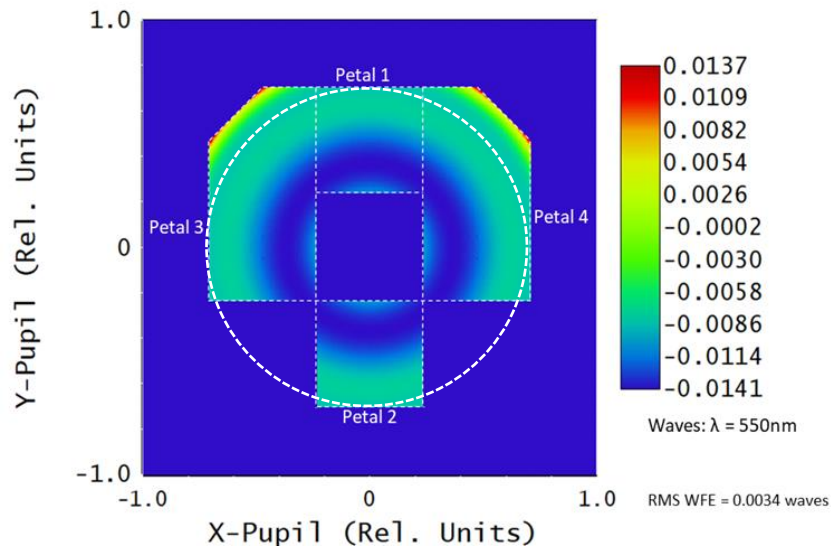


Figure 3-2: Wavefront map with nominal alignment – indicating pupil shape, petal positions, and a 300 mm circle.

3.3 Nominal performance

The nominal RMS wavefront error (RMS WFE) performance of the optical design is shown in Figure 3-3. At 500 km orbital height a 0.23° half field of view corresponds to a 4 km ground footprint diameter. Values are well below the diffraction-limit. This is important as many additional error sources (thermal load, petal residual misalignments...) will contribute to the final optical quality of the imaging system.

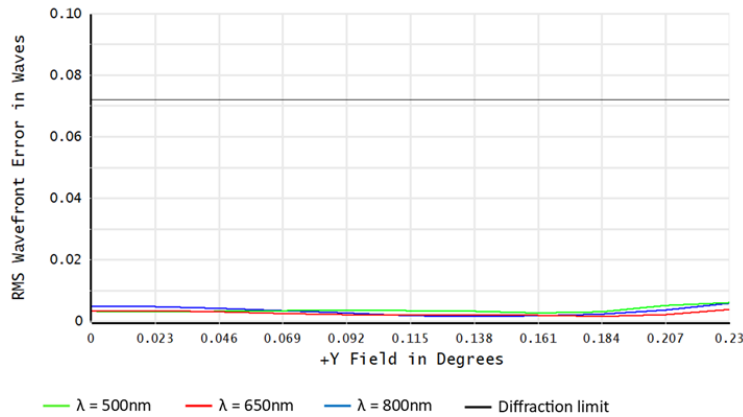


Figure 3-3: Nominal RMS WFE performance for different wavelength as a function of field angle. Values are well below the diffraction-limit (black curve).

Figure 3-4 shows the polychromatic MTF performance of the nominal ISAAC design. A 2D map of the MTF is shown, which demonstrates that the MTF performance is almost but not quite radially symmetric. Given the asymmetry of M1, there is a noticeable difference between the X and Y slices of the MTF.

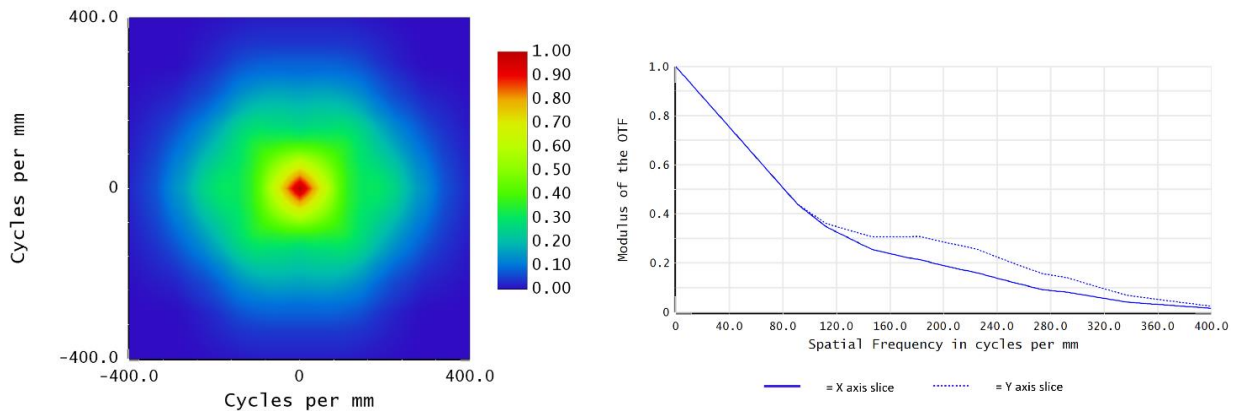


Figure 3-4: Left, polychromatic (500nm-800nm) MTF surface plot; right MTF X and Y slices.

Figure 3-5 shows the polychromatic PSF from 500 to 800 nm for the nominal alignment. Small features, consequence of the pupil shape, are visible but they remain extremely limited. The peaks have little impact on the final image. We have shown in ¹² that these small effects can be mitigated by deconvolution.

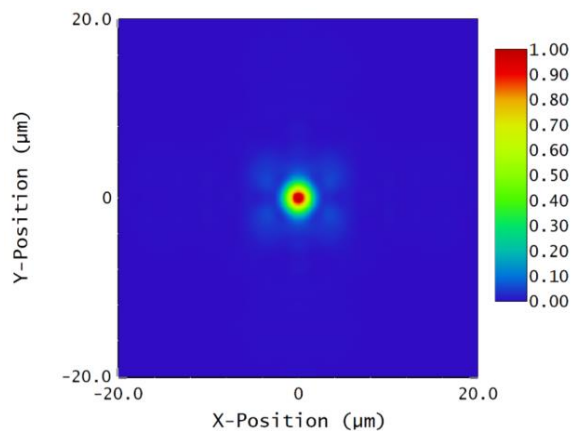


Figure 3-5: Polychromatic (500 to 800 nm) PSF for the nominal alignment.

3.4 Tolerance analysis

To have a more representative analysis of the optical performance of ISAAC, a tolerance analysis was completed. This gives a better sense of the ‘as-built’ optical system and more relevant data in assessing the achieved performance of ISAAC. To model this accurately requires consideration of how the optical system will be aligned and to what precision. To do this the MATLAB-Zemax Application Program Interface (API) was utilised. This enables a custom tolerance analysis that sequentially follows a representative alignment plan, whilst drawing on the optical modelling and analysis tools of Zemax.

A Monte Carlo analysis was performed, whereby each Monte Carlo run followed the alignment sequence. A Gaussian distribution, clipped at one sigma, was applied to each degree of freedom tolerance for each optic. This gives a more representative model of actual achieved tolerances. For example, the M2 decentre alignment precision was modelled as a maximum of $\pm 5 \mu\text{m}$. This reflects the achievable alignment precision of the in-house machining process. Realistically, this machining error will not always be $\pm 5 \mu\text{m}$, hence the applied Gaussian distribution. Within the Monte Carlo tolerance script this alignment precision was modelled, including an optimisation routine that replicated the individual degree of freedom alignment ‘search’. For example, should the optimum alignment of M2 decentre be $-29 \mu\text{m}$ and M2 decentre is currently sat at $+5 \mu\text{m}$, with an alignment precision of $\pm 3 \mu\text{m}$, then $-34 \pm 3 \mu\text{m}$ is the best achievable alignment of M2 decentre.

The tolerance script follows the successive order of the alignment plan, enabling the sequential compensation of optics to correct for the non-perfect alignment of prior optics. This process accurately reflects how many optical systems are aligned, and how ISAAC will be aligned. An optimum alignment plan for ISAAC consists of aligning the field corrector system as an independent sub-system, before aligning the field corrector as a whole with the telescope optics. In the interests of minimising the need for high-precision optical alignment, 6 of the 7 lenses of the field corrector can be placed in a lens barrel with relaxed tolerances – relying just on mechanical positioning and no further alignment steps. The last lens in the lens barrel can be used to correct for the majority of the misalignments of the first 6 lenses.

The telescope itself requires an intricate alignment sequence. First, the fixed M1 petal (petal 1) can act as a reference point of which the deployable petals can be aligned to. Petal 1 must still be close to its nominal alignment, such that it aligns mechanically with the rest of the CubeSat structure. The piston, tip and tilt of the deployable petals are controlled by high precision actuators, and as such can be aligned to sub-micron accuracy in these degrees of freedom (DoF). The decentre of each M1 petal is one of the most sensitive degrees of freedom but can be somewhat compensated by the high accuracy tip, tilt, and piston of the actuated degrees of freedom. Perfect compensation would be possible if M1 were spherical, however as M1 is parabolic then compensation is only partially possible.

Once petal 1 is aligned, the deployable petals can be aligned in 5-DoF to produce a common image location with common performance. M2 can next be aligned, which is actuated to a high precision in tip, tilt, and piston. Decentre of M2 must be aligned using machining or shimming. The alignment of M2 can be determined by measuring the Zernike polynomials interferometrically and comparing to model expectations. Another feasible technique for determining the alignment of the telescope as a whole would be to use a CMM (Coordinate Measuring Machine), which could determine the positions of optics to the micron level – within the required alignment accuracy of ISAAC. M2 alignment, as well as the alignment of the lens barrel as a whole (i.e., all 7 lenses simultaneously), can then be used to optimise the final image performance on the detector.

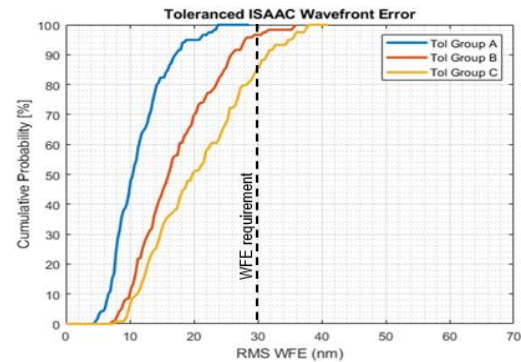
The tolerance results are presented as cumulative probability. This reflects the statistical nature of the Monte Carlo analysis and enables a confidence level on the likelihood of aligning ISAAC with a specific final wavefront error. The wavefront error due to tolerancing is only part of the ISAAC wavefront error budget but is one of the largest contributors.

3.5 Performance after tolerancing

The input tolerances for this tolerance analysis are shown in Table 3-1. Different groups of tolerances were explored for the tolerance analysis. Group B are the tolerance shown in Table 3-1. The tolerances used for group A and C are multiples of the tolerances used in group B: group B = $1.5 * \text{group A}$ and group C = $2 * \text{group A}$. Figure 3-4 shows the cumulative probability of the RMS WFE for each of the tolerance groups. Tolerance group B is able to achieve an overall WFE below 3 nm RMS 97% of the time and appears to be a good compromise.

Table 3-2: Tolerances for group B (Left). Cumulative probability wavefront error (right).

Optic	dX ($\pm \mu\text{m}$)	dY ($\pm \mu\text{m}$)	dZ ($\pm \mu\text{m}$)	rX ($\pm ^\circ$)	rY ($\pm ^\circ$)
Petal 1 (fixed)	7.5	7.5	7.5	0.009	0.009
Petal 2 (deployable)	7.5	7.5	0.01	1.15E-05	1.15E-05
Petal 3 (deployable)	7.5	7.5	0.01	1.15E-05	1.15E-05
Petal 4 (deployable)	7.5	7.5	0.01	1.15E-05	1.15E-05
M2	7.5	7.5	0.01	1.43E-05	1.43E-05
L1-L6	30	30	30	0.138	0.138
L7	7.5	7.5	7.5	0.035	0.035
Whole lens barrel	7.5	7.5	7.5	0.017	0.017



4 MECHANICAL DESIGN OF M1

4.1 6U telescope M1 design

The design work in accommodating a 6U telescope has resulted in a change and optimisation of the M1 design from previous development work^{1,4,12} but is still based on the same fundamental principles. Notable changes/optimisation work has included:

- M1 segment sizes have been optimised to increase the light collecting area, improve pupil dilution, as well as angular resolution in some specific directions.
- Reduction of the number of deployable petals from four to three.
- Deployable M1 petal mounting method has been adjusted to make compatible with CubeSat space environment and requirements.
- Motor sizing has been re-evaluated and requirements set accounting for mechanism uncertainty factors such as resistive frictional forces.

Error! Reference source not found. shows an overview of the 6U telescope M1 design. A predominantly Aluminium Alloy structure is maintained, including mirrors, to ensure any differential thermal contraction effects are minimised.

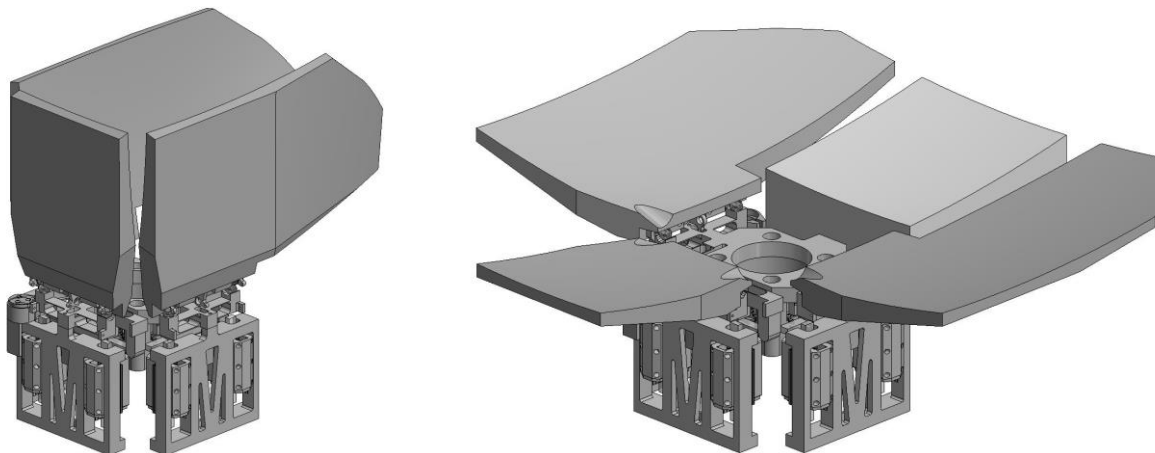


Figure 4-1: Overview of 6U telescope M1 design. Left: Stowed configuration fitting into 3U (L shape). Right: Deployed configuration after launch producing a 300 mm optical aperture.

Deployment of M1 petals is provided by extension springs which, when fully deployed, are in free form state such that forces are not induced on to the petals interfering with the active adjustments. Spring deployment mechanisms can cause undesirable shock or vibration issues when released. These undamped motions can cause repeatability issues in precision

mechanisms. To prevent this from happening the mirror motion is controlled using a Shape Memory Alloy (SMA), in this case Nitinol wire^{1, 11}.

Three motors enable each deployable petal to be further manipulated in tip, tilt, and piston. Within a small envelope, the motors are required to provide nanometre positioning resolution, relatively high actuation forces (in the tens of Newtons) and have the ability to hold position when powered off.

4.2 Actuator testing

Following the updated M1 deployment and petal actuation configuration, it was deemed that component level characterisation of motor performance would be valuable in developing the overall telescope design. The resolution and repeatability of motor actuation can be impacted by the load and the control instrumentation/method. A dedicated actuator test rig has been designed and manufactured (Figure 4-2) to obtain empirical performance characteristics of motors, which were selected as being suitable for M1 petal actuation following a criteria trade-off study. Some select key motor criteria are summarised in **Error! Reference source not found.**

Table 4-1: M1 petal motor criteria.

Criterion	Value	Comments
Resolution	<10 nanometre	Driven by optical tolerance requirements.
Force	>10 Newtons	Driven by mechanism motor sizing.
Vacuum compatibility	Compliant or can be modified to be made compliant	Driven by operational environment.
Operational temperature range	-30°C to 70°C	Driven by environment.

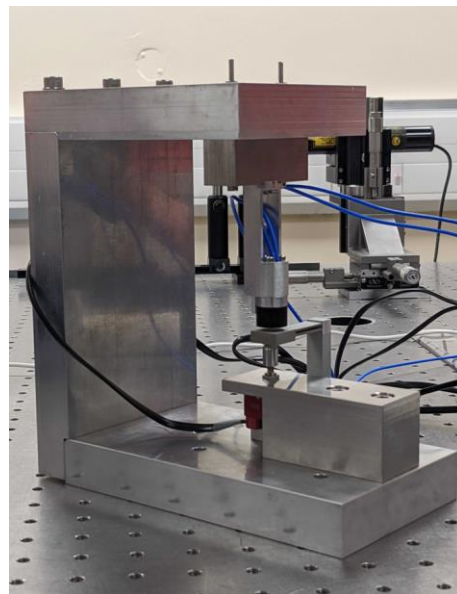


Figure 4-2: Actuator Test Rig; under load configuration.

The test rig allows for actuation displacement to be measured, with the motors both unloaded and loaded, using capacitive sensors capable of sub nanometre resolution. Impact of temperature change on displacement measurements has been minimised by employing a thermally compensated design via material selection and dimensioning. Temperature monitoring will allow a trends/impact on displacement measurements to be characterised. A MATLAB script with control drivers moves the actuators to pre-defined increments and records the sensor displacement measurements. Characterisation of motor performance at component level will make system level testing easier to analyse. Testing is due to be completed in Q3 of 2022.

5 ACTIVE OPTICS

We ensure the final optical quality of the telescope by using active optics. This allows the measurement of the optical aberrations and subsequent correction using the actuators of M1 and M2. The overall wavefront error budget¹³ shows that the residual tip-tilt and pistons for the deployable primary segments and secondary mirror need to be smaller than 20 nm RMS to achieve diffraction-limited imaging the visible and near infrared.

The amplitude of the error terms varies between a few microns (after the initial telescope deployment) down to a few tens of nanometres to ensure a phased telescope. Such a large range drives us to consider different solutions to ensure the alignment, coarse phasing, and fine phasing. The table below summaries the phasing steps and respective methods implemented. Multiple approaches have been studied for the final two phasing steps. Results on the performance of the deployment and phasing step can be found in ^{1, 4, 12}.

Table 5-1: Summary of the phasing steps and method used.

Step	Capture range	Precision requirements	Method
Telescope initial deployment	Folded mirror segments	Within the detector FoV (typ. approx. $\pm 5 \mu\text{m}$)	Extension springs controlled using Shape Memory Alloy (SMA)
Alignment and Coarse phasing	Detector FoV	Sub-wavelength (typ. approx. $\pm 500 \text{ nm}$)	Calibrated displacement sensors Blob detector Image sharpness Machine Learning
Fine phasing	Sub-wavelength	<20 nm RMS	Phase diversity Image sharpness Machine Learning

Some of the aforementioned strategies require the satellite to point at a star for phasing step with a precision and stability that is possible with currently available technology. The typical alignment and phasing sequence procedure is presented Figure 5-1. Using a star as reference, Figure 5-2 shows the typical duration for the complete phasing of the telescope which should take between 0.3-60s depending on magnitude of the star used on the number of measurements required to achieve the image quality. This is in line with current state of the art and envisioned orbits and enables measurements with good signal-to-noise ratio. The number of images required will depend on the algorithms, e.g., a minimum of two for phase diversity, but often more for image sharpness. We show in ³, that only a few images (iterations) are necessary to achieve the desired image quality.

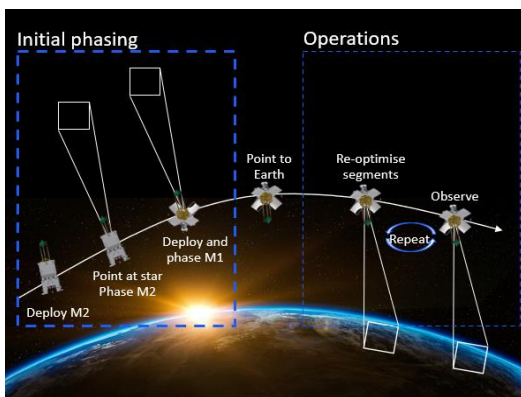


Figure 5-1: Illustration of the potential alignment and phasing sequence.

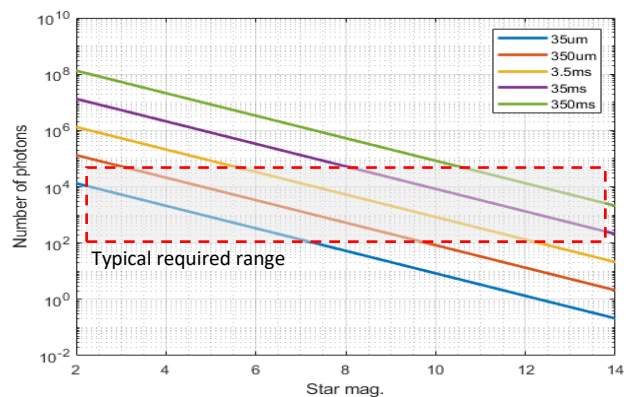


Figure 5-2: Typical number of photons as a function of star magnitude and integration time.

For the coarse phasing, and as a complementary strategy to using the on-board displacement sensors¹⁴, we propose the use of a “blob” detection algorithm to perform the coarse phasing step. This method has the advantage of only relying on the detector images (i.e., where the final optical quality is required) without the need of a mechanical calibrated reference. In the blob detection algorithm, each petal is dithered individually using a small motor movement and a new image is taken (see Figure 5-3 and Figure 5-4). The difference between the new and previous images is computed. Finally, the PSF which

belongs to the petal being addressed is identified and the petal is moved accordingly to align the PSF with the centre of the field of view. Preliminary simulation results show that tip-tilt (i.e., optical alignment) can be achieved with very high accuracy, with tip-tilt residuals of 50 nm RMS on average for bright stars. Five images are necessary to compute the differential images for the 4 petals, with a final image after alignment used for validation. Increased stability and robustness in terms of linear behaviour of the actuators or field distortions can be obtained by using small gain values, which would require more images. This leads to a trade-off between the number of images required and the final performance.

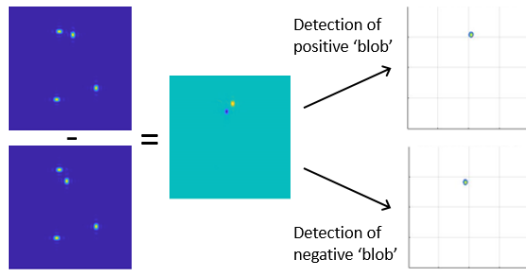


Figure 5-3: Principle of blob detection in differential image.

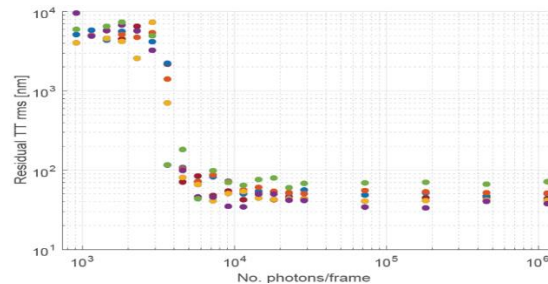


Figure 5-4: Tip-tilt residual after correction as a function of flux (RON=10, single iteration alignment).

Finally, the coarse and fine phasing steps can be addressed by machine learning techniques. Initial results using a VGG Very Deep Convolutional Network are promising on a point-source³ and has the potential to allow correction during observation using the extended ground images.

6 CONCLUSION

In this paper we presented a concept for a very high-resolution Earth Observation CubeSat using deployable primary mirrors. The objective of this technology is to provide very high-resolution optical imaging from low Earth orbit at low-cost. This is achieved by folding a large 30 cm+ telescope into a small volume - typically in a 6 CubeSat - for launch. We have demonstrated by design that we can package all elements of the satellite (i.e., payload and bus / platform) in the extremely limited 6U CubeSat volume to fit a 30 cm+ aperture. The optical design has demonstrated excellent wavefront quality and we have shown that a realistic alignment plan can meet the tight optical requirements. UK ATC's initial proof-of-concept developments demonstrated in laboratory that it is possible to fit the mirrors and structure within the exceedingly small CubeSat volume, to deploy M1 segments with a precision of several microns, and to control their position with a precision of several tens of nanometres. We have also demonstrated excellent position control thanks to embedded displacement sensors, allowing for precise alignment of the mirror segments. Finally, we have validated the self-alignment procedure using numerical simulations, which now need to be tested in the laboratory. Testing of the fine motion actuators is on-going and is due to be completed in Q3 of 2022.

ACKNOWLEDGMENTS

This paper describes work that was performed within the CLASP (Challenge Led Applied Systems Programme) scheme grant entitled "ISAAC - Integrated Space Active Optics for Aberration Compensation". The United Kingdom Astronomy Technology Centre was awarded funding through the United Kingdom Science and Technology Facilities Council STFC (Grant no. ST/V002309/1).

REFERENCES

- [1] Schwartz, N., et al., "A segmented deployable primary mirror for earth observation from a CubeSat platform," in Proc. AIAA/USU Conf. Small Satellite, vol. SSC16, p. SSC16-WK-23 (2016).
- [2] Sauvage, J.-F., et al. "Opto-mechanical model of AZIMOV, the deployable telescope for CubeSat," Space Telescopes and Instrumentation 2022: Optical, Infrared, and Millimeter Wave, Proc. SPIE12180, 12180-8 (2022).
- [3] Dumont, M., et al. "Deep learning for space-borne focal plane wavefront sensing," Space Telescopes and Instrumentation 2022: Optical, Infrared, and Millimeter Wave, Proc. SPIE 12180, 12180-236 (2022).

- [4] Schwartz, N., Brzozowski, W., et al., "High-resolution deployable CubeSat prototype," Proc. SPIE 11443, Space Telescopes and Instrumentation 2020: Optical, Infrared, and Millimeter Wave, 1144331 (2020).
- [5] Gooding, D., et al. "A novel deployable telescope to facilitate a low-cost <1m GSD video rapid-revisit small satellite constellation." International Conference on Space Optics—ICSO 2018. Vol. 11180. International Society for Optics and Photonics, (2019).
- [6] Cappelletti, C., Battistini, S., and Malphrus, B. (Eds.). "CubeSat Handbook: From Mission Design to Operations". Academic Press, (2020).
- [7] Hancock, S., et al., "Working towards spaceborne lidar with wall-to-wall coverage: photonics and deployable optics," Proc. SPIE 11888, Space, Satellites, and Sustainability II, 1188805 (2021).
- [8] Liu, Hua, and Qihao Weng. "Enhancing temporal resolution of satellite imagery for public health studies: A case study of West Nile Virus outbreak in Los Angeles in 2007." Remote Sensing of Environment 117 (2012): 57-71.
- [9] Sadeh, Yuval, et al. "Fusion of Sentinel-2 and PlanetScope time-series data into daily 3 m surface reflectance and wheat LAI monitoring." International Journal of Applied Earth Observation and Geoinformation 96 (2021).
- [10] Walker, Jeffrey, and Paul Houser. "Soil moisture estimation using remote sensing." Proceedings of the 27th Hydrology and Water Resources Symposium, (2002).
- [11] Patent "A moveable joint" (granted 10 June 2020).
- [12] Schwartz, N., et al., "Laboratory demonstration of an active optics system for high-resolution deployable CubeSat," in 4S Symposium, vol. 1, pp. 1–15 (2018).
- [13] Sauvage, J.-F., et al. "AZIMOV: First error budget of a deployable CubeSat telescope," Space Telescopes and Instrumentation 2020: Ultraviolet to Gamma Ray. Vol. 11444. International Society for Optics and Photonics, 2020.
- [14] Razorbill Instruments <<https://razorbillinstruments.com/zed-cap-a-compact-high-precision-displacement-sensor/>> (01 July 2022).
- [15] Villalba, V., Kuiper, H., Eberhard Gill, "Review on thermal and mechanical challenges in the development of deployable space optics," J. Astron. Telesc. Instrum. Syst. 6(1), 010902 (2020).